

RESEARCH ARTICLE

Improvement of Power System Frequency Stability With Universal Grid-Forming Battery Energy Storages

HANNU LAAKSONEN^{ID}, (Member, IEEE)

School of Technology and Innovations, Flexible Energy Resources, University of Vaasa, 65200 Vaasa, Finland

e-mail: hannu.laaksonen@uwasa.fi

ABSTRACT Large-scale integration of inverter-based renewable generation leads to the reduction of power systems' natural inertia. Therefore, the dynamics of the future power systems will be more sensitive than in the traditional systems with high-inertia rotating synchronous generators. This development is a potential risk for frequency stability and requires utilization of rapidly controllable resources for dynamic frequency stability support. Simultaneously, development of new synchronization and control methods for inverter-based resources is needed in order to ensure the frequency and synchronization stability of future power systems. In this paper, a grid-forming and supporting universal frequency-locked-loop -based control and grid synchronization for inverter-based resources is utilized to improve the frequency stability of a small high-voltage network. The simulations are done with PSCAD software and the main focus is on the battery energy storages to evaluate the effect of their location, enhanced control schemes as well as operation mode on frequency stability. In the studies, for example, the effect of battery storages location, active power response related control parameters, communication time delay and input frequency determination on frequency support are studied during charging and discharging of the batteries. Based on the simulations, also new solutions to improve the frequency stability of future variable inertia power systems with universal grid-forming battery storages are proposed.

INDEX TERMS Frequency stability, inverter-based resources, grid-forming, battery energy storages, power systems.

I. INTRODUCTION

A. BACKGROUND

Due to large-scale deployment of renewable energy sources (RES), inverter-based resources (IBRs) have been replacing traditional synchronous generators (SGs) in the power systems. RES-based IBRs, like wind and photovoltaics (PV), are connected to the power system through power electronic interfaces without natural kinetic inertia. This reduces power system rotational kinetic energy i.e. system inertia as well as changes dynamic behavior after major disturbances. In general, inertia stabilizes power system and resists changes in system frequency. Therefore, larger variations in frequency

and rate of change of frequency (ROCOF) are possible due to reduced inertia and there is an increased risk to lose the frequency stability of the power system after a large disturbance. Without utilization of rapidly controllable resources and technologies, like battery energy storage systems (BESS) and future-proof IBR control schemes, reduced system inertia could prevent full-scale deployment of RES. BESSs can be used to support the frequency stability and post-disturbance frequency swing with fast frequency response (FFR) control service, for example, by using their active power-frequency (P_f) -droop functionality. However, FFR operation is based on measured frequency which creates some delay to its active power response and frequency support. In addition, the frequency stability of future low inertia power system will be determined largely by the control and synchronization

The associate editor coordinating the review of this manuscript and approving it for publication was Siqi Bu^{ID}.

methods of IBRs and their stability as well as other features. The effect increases when the share of IBRs in the power system with different grid-following (GFL) and grid-forming (GFM) control schemes is high compared to the SG-based generation. References [1], [2], [3], [4]

B. CONTROL SCHEMES FOR INVERTER-BASED RESOURCES

In this Section I-B different 1) GFL and GFM as well as 2) active (P) and reactive power (Q) related control schemes of IBRs, like BESS, are briefly reviewed.

1) GRID-FORMING AND GRID-FOLLOWING CONTROL METHODS

Grid-following GFL inverter is often described as a controlled current source with high parallel impedance and grid-forming GFM inverter as a voltage source with low series impedance [5], [6]. There is no generally accepted definition for GFM control [5]. Synchronization principles of GFL and GFM inverters are one of the key differences between them. Commonly a GFL inverter uses voltage-based network synchronization [7] which means that it is synchronized to measured or estimated network voltage angle, for example, by phase-locked-loop (PLL) or frequency-locked-loop (FLL) component. On the other hand, most GFM inverter control methods do not require a PLL or FLL. GFM control methods can be based e.g. on power synchronization [7], [8] to emulate the power synchronization principles of SGs [5]. Droop-based grid-forming control schemes and power synchronization control are the most commonly used GFM control schemes and can be also seen quite similar to each other [7]. In the literature, many different GFM control methods have been proposed and presented in [5], [7], [9], and [35], like

- 1) Droop-Based Grid-Forming Control Methods (e.g. the basic droop control and the droop control using low-pass filter),
- 2) Power Synchronization Loop / Power Synchronization Control (PSC)
- 3) Voltage Controlled Inverter (VCI)
- 4) Virtual Synchronous Machine (VSM) / Virtual Synchronous Generator (VSG)
- 5) Virtual Oscillator Control (VOC) / dispatchable Virtual Oscillator Control (dVOC)
- 6) Matching Control
- 7) PLL-Based Modified Current-Controlled Methods
- 8) Direct Power Control (DPC) and
- 9) Motor-generator pair (MGP) [35].

One key difference between GFL and GFM behavior is in their response to a network disturbance as well as in their small-signal operation when connected to a weak or stiff grid [5]. More information about advantages and disadvantages of GFL and GFM control methods can be found from [10]. In [35] also summary about advantages and disadvantages of different GFM control methods (i.e. droop-

control, VSG and MGP) has been done by comparing their transient response and frequency stability.

2) ACTIVE AND REACTIVE POWER CONTROL SCHEMES

Fast frequency response, FFR, does not have commonly agreed exact definition either. Therefore, for example, in [1] it is defined as “any type of rapid, active power increase or decrease by generation or load, in a time frame of less than 2 seconds, to correct frequency imbalances and to assist with managing the system frequency.” As stated previously, for example, BESS can provide FFR service by its Pf -droop functionality. However, FFR and virtual or synthetic inertia services of IBRs have the challenge or drawback, when compared to natural kinetic inertia provided by SG-based units, that their response is delayed and affected by the associated frequency or ROCOF measurements. For example, measurement time windows of 100 ms and 500 ms can significantly impact these measurements [1]. Due to this small time delay during the initial period of frequency change after disturbance), the FFR or synthetic inertia service and support impact of IBR is missing [1]. Some classification of frequency control related ancillary services based on their response times and duration can be found, for example, in [1] and [11]. In Nordic power system, the response time requirements for fast frequency reserve services are between 0.7 s and 1.3 s depending on the magnitude of the under-frequency. In the literature, also improvements for estimating the frequency or ROCOF in low inertia power system has been presented. For example, [12] proposed more accurate ROCOF estimation algorithm based on least square method with flexible window size and median filter.

Amongst the various DER and IBRs, BESSs are expected to play an important role in future smart grids due to their fast and controllable dynamics and potential to provide multiple different flexibility services in stationary applications. In the literature, different frequency control related services, like FFR, provision by BESSs have been studied and these services are typically realized either by an individual large-scale BESS or by aggregating multiple small-scale BESSs [13], [14]. In addition to FFR service, BESSs can also provide other active (P) and reactive power (Q) related flexibility services which can be realized by various inverter local control modes or functions. For example, functions such as constant power factor ($\cos\phi$), fixed Q , $Q(P)$, $\cos\phi(P)$, QU , PU and Pf , where f is frequency and U is voltage, are required by different grid codes. References [1], [3], [15], [16]

C. STABILITY OF FUTURE POWER SYSTEMS WITH IBR

Power system stability can be defined as the ability of a power system to maintain acceptable state and recover balance after a disturbance. The main state variables are power system frequency, bus voltages and the rotor angles of SGs. Therefore, stability has been traditionally categorized into frequency, voltage and rotor angle stability [17]. Frequency stability is not the only stability concern, but it has been recognized as

one of the major system-level stability issue in the future RES- and IBR-based low inertia power systems. In general, frequency stability means that the power system frequency does not deviate too much from the nominal frequency. Related to this, there exists different factors which determine the frequency stability like i) generator inertia (larger value slows down frequency change), ii) load inertia and load damping (larger value slows down frequency change), iii) contingency size (larger value increases frequency change), iv) under-frequency protection settings of load shedding (UFLS) and v) frequency response speed (faster and larger response slows down frequency changes). Options to maintain the frequency stability include, for example, I) maintaining the inertia of the system (e.g. SG-based generation or synchronous condensers), II) providing more response time (reduced contingency size or reduced UFLS settings), III) fast active power-frequency (P_f) response (e.g. by IBR-based resources like BESSs with GFL control and load demand response) or iv) providing synthetic inertia and synchronization stability from GFM IBRs. References [2], [3]

The local frequency measurement determines the frequency response of the generators and loads after disturbance. In the future large IBR-based power systems the remaining natural inertia may be distributed on some parts of the system and therefore, depending on the location or region, the ROCOF and frequency values after disturbance can deviate more than in traditional SG-based systems with high inertia [1]. Therefore, also services for fast frequency support should be distributed across the power system. In addition, the increasing amount of IBRs in the future power systems requires also new stability definitions [18]. The frequency stability will be increasingly defined by the control and synchronization methods of IBRs and their stability. The effect of IBRs is higher when their share with GFL and GFM control is large when compared to the SG-based generation. Therefore, it is valuable to know what amount of generation comes from IBRs. Typically used metrics have been a) the percentage of inverter-based generation (% IBR) from the total generation or total load and b) system nonsynchronous penetration (SNSP) which includes also e.g. HVDC links. However, both metrics have some drawbacks which are defined in [19] with more details. Therefore, new metric called voltage-forming ratio, where the total grid-forming IBR capacity and also type of GFM control scheme is considered, have been proposed in [19]. Voltage-forming ratio could be defined as the ratio of the voltage-forming capacity (synchronous generators, synchronous condensers, and GFM IBRs) to the total apparent power capacity (synchronous generators, synchronous condensers, and all IBRs) [19].

In [20] large-scale deployment of GFMs was studied from frequency stability viewpoint. It was suggested that with sufficient controller tuning, it is possible to guarantee frequency stability. However, due to more sensitive dynamics than in traditional SG-based system, frequency nadir and ROCOF change should be carefully considered in certain protection

and load shedding schemes as well as power system stabilizer (PSS) settings. Faster frequency variations can also be a potential challenge for existing GFL-based resources and their stability. Reference [20] In addition to GFM control, also other services, like FFR with fast active power control, will be needed to ensure frequency stability of power systems with very high-share of IBRs. Typical GFM controlled IBR is capable of providing FFR, but often it may be dispatched to maintain controllability for FFR provision (i.e. curtailed operation of variable generation GFM to enable up-regulation with FFR). Reference [19]

In a low inertia transmission network, the possible interactions of control schemes of large-scale IBRs with other power system components needs to be studied before their interconnection and also monitored during the real-time operation. For example, wind power plants connected to series compensated transmission network may increase risk of sub-synchronous oscillations. Reference [21] In transmission system level stability studies, it is crucial to consider the transmission line dynamics and their possible mutual effects, for instance, with GFM-based control methods [22] as well as take into account the grid topology and actual location of IBRs in the grid [4]. In addition, the dynamics of various IBR-based loads, like electric vehicles charging, BESS charging, hydrogen electrolyzers [23], and their mutual effects should be considered as part of future stability analysis which may also require development of new stability theory for power systems with high share of IBRs [4]. Therefore, in order to find out the IBRs which are causing the oscillations, in [24] a reversed impedance-based stability criterion for IBR-based power systems was proposed. Proposed new criterion of [24] enables the study of system-wide oscillation modes created by control interactions of multiple IBRs integrated in large power systems.

Large-scale implementation of IBR-based generation in the future power systems requires also constant updates on grid codes. Grid codes need to pay more attention to GFM-based inverters' capabilities and challenges as well as also, for example, notice that full reactive current injection during major grid faults may cause loss of synchronization of IBR-based generation. Reference [7] On the other hand, it is still unclear how to best represent multiple IBRs with different control schemes in bulk power system simulations [25]. Related to this, more research on the small-signal synchronization stability of GFMs is needed and instead of design-oriented analysis, which are more applicable to single IBR systems, new reduced-order or data-driven modeling methods for future power systems with huge amount of IBRs are needed [26]. Further development of tools like real-time simulators [27] and grid emulators is also highly important. New modeling methods for multiple GFMs and GFLs have been presented e.g. in [28]. Reference [29] also emphasized the need of an effective system analysis tool, which can identify the oscillation modes of multiple IBRs from different vendors as well as system partitioning methods and dynamic model

aggregation techniques for the stability analysis of very large IBR-based power systems. In addition, [30] discussed about the classification and characterization needs of IBRs with different control schemes based on their transient different behavior in response to grid disturbances.

Role of grid emulator functionalities becomes very important when new inverter control schemes are tested before the real-life implementation [31]. Grid emulator needs to be able to represent future low or variable inertia power systems with different share of IBRs and SG as well as emulate also the different shares of GFM- and GFL-based IBR generation. In addition, also the ability to model the dynamic behavior of IBR-based loads, becomes increasingly important to see the potential mutual effects between various control schemes during different type of variations and disturbances. It is also commonly agreed that the development of appropriate processes for testing and validating the capabilities of the GFMs is rapidly needed [11]. In [32] an experimental verification about the ability of GFM inverters to stabilize a transmission network was presented by performing power hardware-in-the-loop (PHIL) simulation to connect a large-scale BESS to a real-time electromagnetic transient (EMT) simulation of future Maui power system. Reference [33] also highlighted the importance of the DC dynamics modelling with detailed DC source models in GFM control design as well as the critical need for an effective AC current limitation scheme by studying potentially destabilizing interaction between the fast synchronization of GFMs and the slow response of SGs.

D. OBJECTIVES AND ORGANIZATION

In the future low-inertia power systems with high-share of IBRs, for example, following features are needed:

- Increased amount of GFM-based resources with advanced control features to support frequency and synchronization stability in systems with variable share of SGs and GFL/GFM IBRs,
- Frequency stability supporting services from GFL and GFM IBRs, like BESSs, based on their rapid active power control i.e. FFR and virtual or synthetic inertia services with minimized response delay,
- Consideration of transmission network lines and location of resources providing frequency stability supporting FFR services and control schemes of GFM-based IBRs in detail in order to avoid negative mutual effects,
- Develop enhanced GFM control schemes which e.g. do not require operation curtailment when providing FFR services and
- Take into account the possibility of IBR-based loads to support frequency and synchronization stability with their advanced control schemes.

In this paper, the grid-forming and supporting universal frequency-locked-loop (U-FLL)-based control and grid synchronization for IBRs [10] is utilized when the effect of different control methods of IBRs are studied with PSCAD simulations using simple transmission network model. Regarding

to the U-FLL, the target is that it would be applicable to different type of future variable inertia power systems with different share of rotating SGs and IBRs. GFM-based IBR with U-FLL does not required operation curtailment when providing FFR services. Main focus in the simulations is especially on the role of BESSs and on the effect of their location, control scheme as well as operation mode (charging or discharging) on frequency stability support. In the studies with BESSs in discharging mode, the Pf - and reactive power-frequency (Qf)-control schemes are compared. In addition, the effect of BESSs location, Pf -droop parameters, communication time delay and input frequency determination on BESS Pf -control based frequency support are studied during BESS charging and discharging in order to improve FFR service of GFM-based BESSs. New solutions which can improve FFR response of GFM-based IBRs and support frequency stability of future variable inertia power systems are proposed based on the simulations.

In the following, Section II presents very briefly the grid-forming/-supporting U-FLL synchronization method for IBRs. Then, Section III presents the study cases and simulation models with different shares of IBRs and SGs in HV hybrid power systems as well as with 100 % IBR-based HV networks. Thereafter, the simulation results are presented in Section IV and conclusions are stated in Section V.

II. UNIVERSAL GRID-FORMING IBR CONTROL AND GRID SYNCHRONIZATION METHOD

Currently there does not exist any universal GFM control and synchronization method. Therefore, a new universal grid-forming/-supporting U-FLL-based synchronization (Fig. 1) for IBRs was proposed in [10].

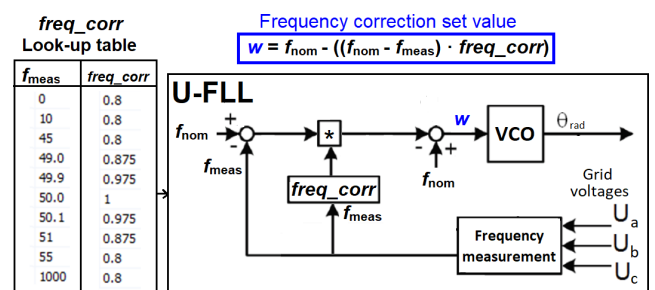


FIGURE 1. Proposed universal grid-forming and supporting U-FLL synchronization method.

More information about the general targets and related issues as well as details of U-FLL can be found from [10].

III. STUDY CASES AND SIMULATION MODELS

The main study cases of this paper are summarized in Table 1. The main simulation cases (Table 1) included:

- a) DER units with U-FLL -component (Fig. 1) for grid synchronization (instead of traditional PLL)
 - o 4 MW BESS: average models with controlled voltage sources, i.e. without power electronic switches,

TABLE 1. Main study cases.

Case	Voltage level	Type and number of generating units	Synchronization of IBRs
CASE_HV_HYBRID	HV	BESS (16-18), SG (1)	U-FLL
CASE HV IBR	HV	BESS (68)	U-FLL

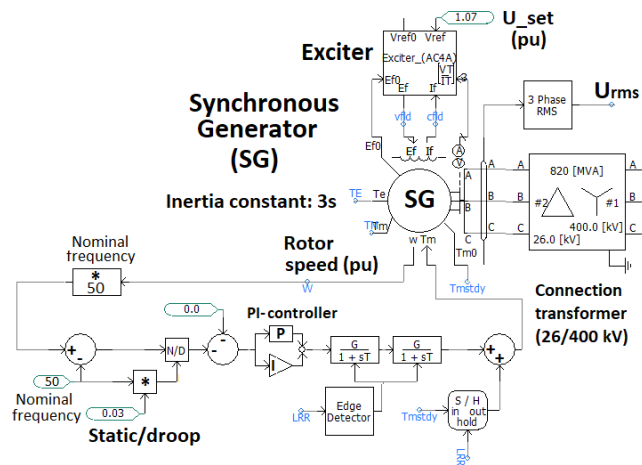


FIGURE 2. SG's (HV network connected) PSCAD model used in CASE_A_HV_HYBRID and CASE_B_HV_HYBRID (Fig. 4).

in order to reduce the needed simulation time, connected in MV network, operation in discharge and charge modes (generation and load) (Fig. 3)

- b) Power system models with different DER locations, control schemes and operation modes
 - o Hybrid power system with IBRs and SG
 - 16 BESSs (MV network, Fig. 3) or 18 BESSs (Fig. 5) and SG (HV network, Fig. 2) in small HV network, BESSs both in discharging (CASE_A_HV_HYBRID), charging (CASE_B_HV_HYBRID) operation (Fig. 4) and 2 BESS (from total of 18 BESSs) at the SG connection point (CASE_C_HV_HYBRID) (Fig. 5)
 - o 100 % IBR-based power system
 - 68 BESSs (MV network, Fig. 3) in small HV network, discharging operation, (CASE_HV_IBR) (Fig. 6)
- c) Following issues were studied and compared in the study cases (see Table 1 and Section IV)
 - o Hybrid system (HV), CASE_A_HV_HYBRID and CASE_B_HV_HYBRID (Fig. 4), CASE_C_HV_HYBRID (Fig. 5)
 - Effect on frequency stability after load change in HV network
 - Effect of BESS Pf- and Qf-droop control (in HV network connected operation reverse Qf-droops are used i.e. reactive power is drawn from the network during under-frequency events and fed to

the network during over-frequency events), BESSs both in discharging (CASE_A_HV_HYBRID) & (CASE_C_HV_HYBRID) and charging (CASE_B_HV_HYBRID) operation

- Effect of location of universal grid-forming/-supporting FLL / IBR-based generation or load with Pf-control on SG stability i.e. near the connection point of SG or at the end of transmission line (close to loads)
- Effect of non-linear Pf-droop (during discharging) with BESS
- Effect of different input frequencies on BESSs Pf-control
- Effect of communication time delay on BESSs Pf-control
- o 100 % IBR-based system (HV), CASE_HV_IBR (Fig. 6)
- Focus on effect of modified 'adaptive' U-FLL coefficient
- Also need to adapt IBR-based DER (BESS) control schemes when transitioning from hybrid to 100 % IBR (CASE_HV_IBR)

IV. SIMULATION RESULTS

In the following, the main simulation results from different study cases (see Section III) are presented. First, in Section IV-A results from small hybrid HV network with discharging of BESSs (CASE_A_HV_HYBRID, Fig. 4 and Table 1) simulations are presented. Next, Section IV-B presents the simulation results from small hybrid HV network with charging of BESSs (CASE_B_HV_HYBRID, Fig. 4 and Table 1). Then, Section IV-C shows the results from cases with small hybrid HV network with two additional BESSs at the connection point of SG (CASE_C_HV_HYBRID, Fig. 5 and Table 1). Finally, in Section IV-D the results from 100 % IBR-based small HV network (CASE_HV_IBR, Fig. 6 and Table 1) are presented.

A. SMALL HYBRID HV NETWORK – DISCHARGING OF BESSs

The total simulation time in Section IV-A subcases was $t = 20.0$ s and 100 MW load increase at the end of 50 km transmission line (Fig. 4) happened at $t = 5.0$ s. Before the load increase in Section IV-A subcases the total load was 505.5 MW, active power generation of each BESS was 3.5 MW and total active power of 16 BESSs was 56 MW. BESS mode change from discharging to charging during frequency oscillations would have improved the frequency stability support, but operation mode change was disabled in the simulations of Section IV-A.

1) A.1 EFFECT OF PF- AND QF- CONTROL

The PSCAD simulation results from case CASE_A_HV_HYBRID (Fig. 4 and Table 1) subcases (Table 2) for studying the effect of Pf- and Qf-control of BESSs are presented in

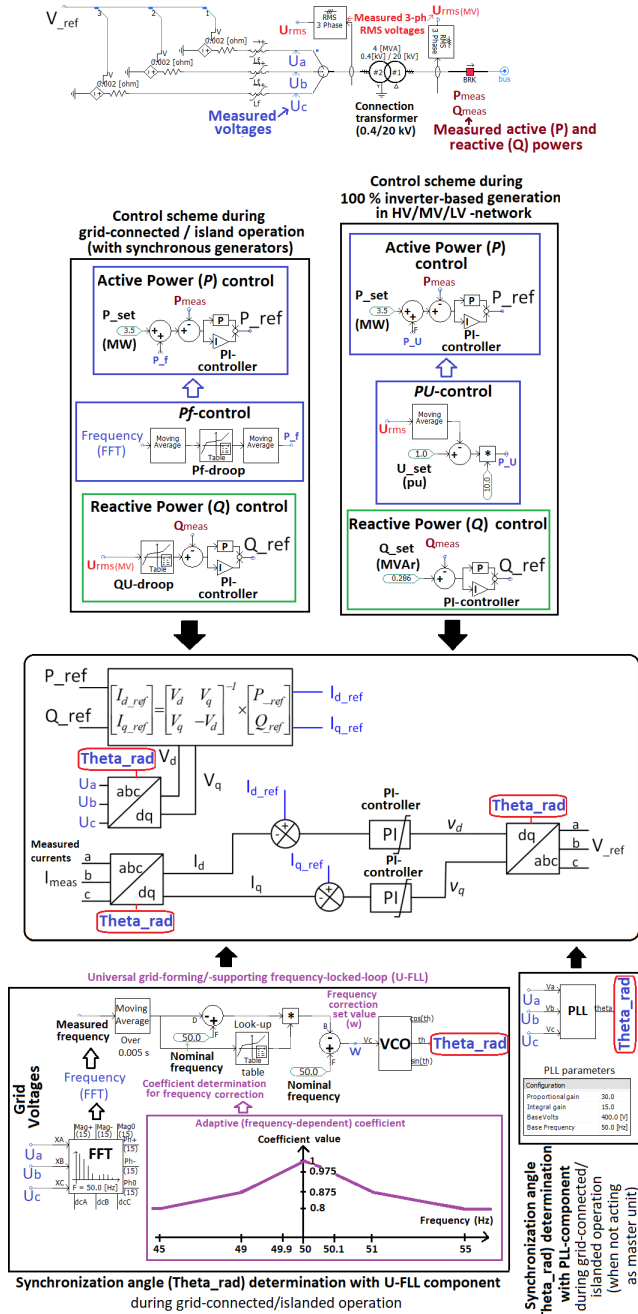


FIGURE 3. BESS's average PSCAD model with controlled voltage sources and control scheme with U-FLL (Fig. 1) or traditional PLL.

TABLE 2. Discharged BESSs' control scheme differences in subcases of CASE_A_HV_HYBRID (Fig. 4, Table 1).

Subcase	BESSs control
CASE_A_HV_HYBRID (U-FLL)	No P_f - or Q_f -control, QU -control
CASE A HV HYBRID P_f (U-FLL) ^(*) , ^(**)	P_f -control, QU -control
CASE A HV HYBRID Q_f (U-FLL)	Q_f -control
CASE A HV HYBRID P_f Q_f (U-FLL) ^(*) , ^(***)	P_f - and Q_f -control

^(*) P_f -control frequency input (Fig. 3) from PSCAD FFT-block with moving average over 100 ms. P_f -control frequency input has also moving average component over ^(**) 100 ms or ^(***) 250 ms after P_f -droop (Fig. 3)

Fig. 9-13. In P_f -control frequency input comes from PSCAD FFT-block and it is moving averaged over 100 ms before and 100/250 ms after P_f -droop (Fig. 3 and 7). Fig. 7 and

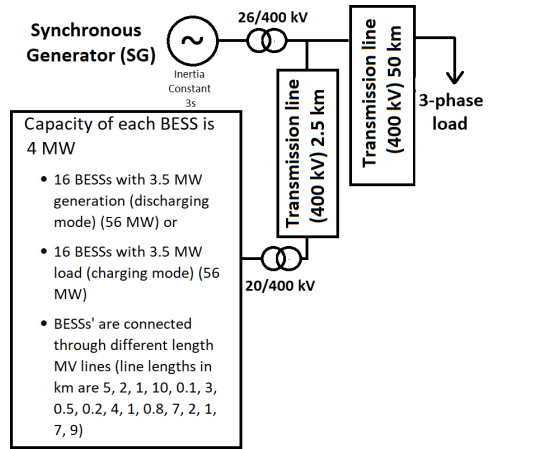


FIGURE 4. One-line diagram of the hybrid small HV network with 16 BESSs (Fig. 3) and SG (Fig. 2) (CASE_A_HV_HYBRID) and (CASE_B_HV_HYBRID).

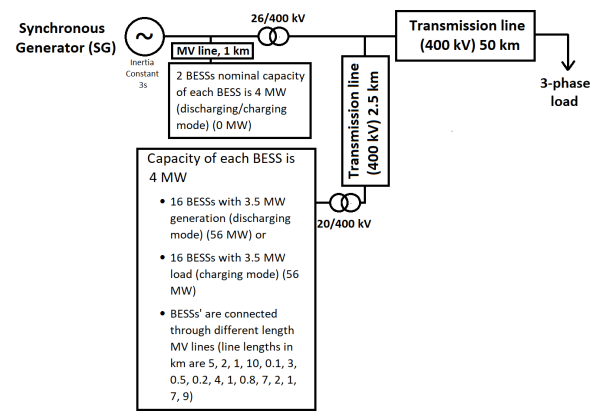


FIGURE 5. One-line diagram of the hybrid small HV network with 2 BESS (Fig. 3) also in SG connection point, in addition to BESSs (MV network) and SG (HV network) (Fig. 4) (CASE_C_HV_HYBRID).

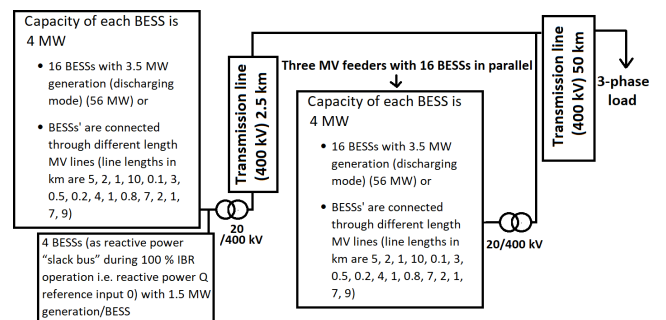


FIGURE 6. One-line diagram of the 100% IBR-based small HV network with 68 BESSs (in MV network, Fig. 3) in CASE_HV_IBR.

Fig. 8 show the control schemes and P_f -, QU - and Q_f -droops of the BESSs which were utilized in subcases (Table 2) of CASE_A_HV_HYBRID. In Fig. 9, the measured frequencies, calculated from the rotating speed of SG (Fig. 2 and 4), after load increase in CASE_A_HV_HYBRID subcases (Table 2) are shown. Fig. 12 and 13 show the total active and reactive power of BESSs in different cases (Table 2).

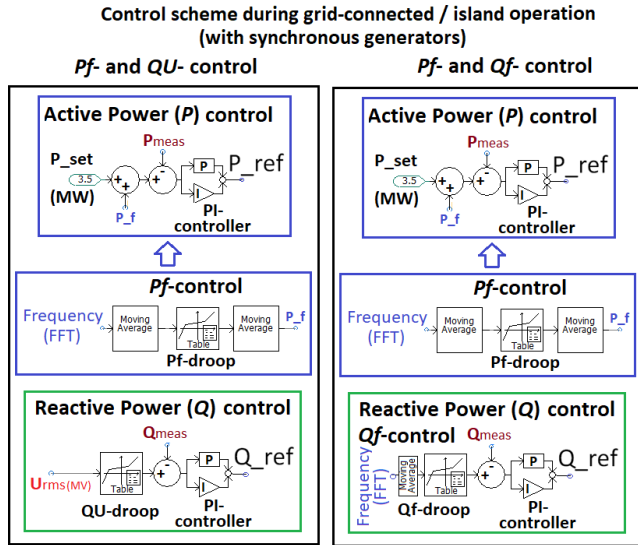


FIGURE 7. BESS's active and reactive power control schemes (Fig. 3, Table 2).

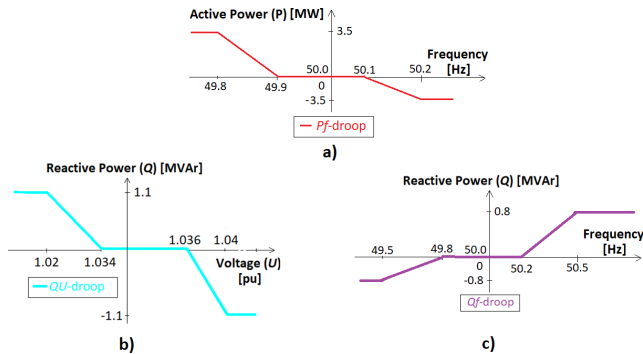


FIGURE 8. BESS's a) *Pf*-droop, b) reactive power-voltage (*QU*-droop) and c) *Qf*-droop settings (Fig. 3, Table 2).

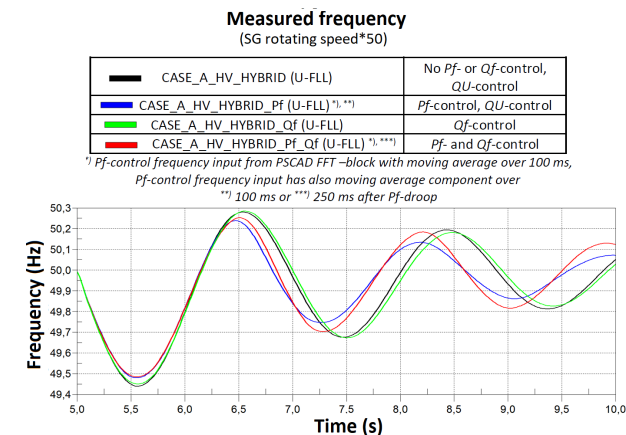


FIGURE 9. Measured frequency calculated from rotor speed of SG after load increase at $t = 5.0$ s with discharged BESSs in *CASE_A_HV_HYBRID* subcases (Table 2).

It can be seen from Fig. 9-11 that the operation of *Pf*-droop control when compared to operation without *Pf*- or *Qf*-control is very beneficial from frequency stability viewpoint after the load increase. Pure *Qf*-control in

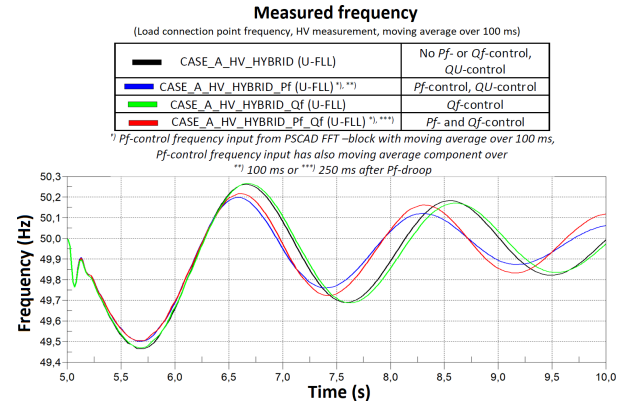


FIGURE 10. Measured frequency calculated from load connection point frequency (100 ms moving average) after load increase at $t = 5.0$ s with discharged BESSs in *CASE_A_HV_HYBRID* subcases (Table 2).

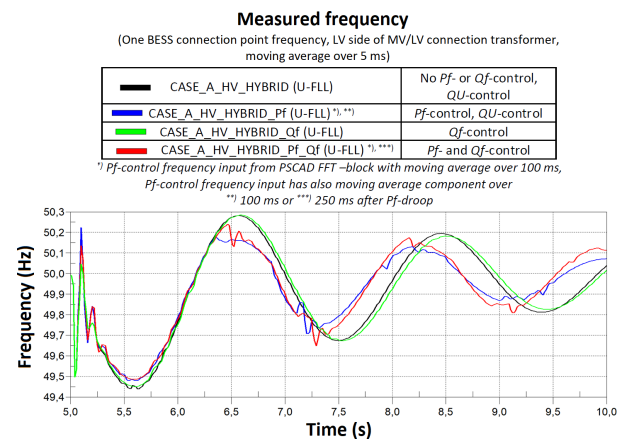


FIGURE 11. Measured frequency calculated from one BESS connection point frequency (5 ms moving average) after load increase at $t = 5.0$ s with discharged BESSs in *CASE_A_HV_HYBRID* subcases (Table 2).

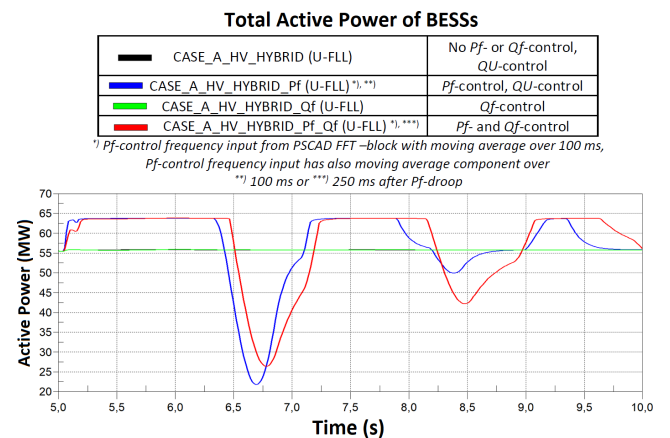


FIGURE 12. Total active power of all 16 BESSs after load increase at $t = 5.0$ s with discharged BESSs in *CASE_A_HV_HYBRID* subcases (Table 2).

CASE_A_HV_HYBRID_Qf (Table 2) makes frequency stability even worse than without it in *CASE_A_HV_HYBRID*. When comparing Fig. 9-11, one can see that there are differences between measured frequencies from different

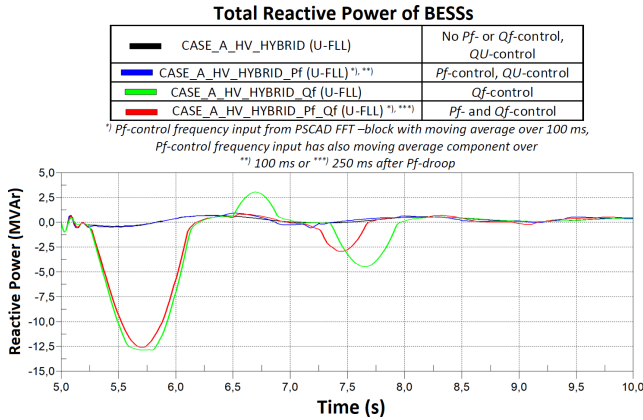


FIGURE 13. Total reactive power of all 16 BESSs after load increase at $t = 5.0$ s with discharged BESSs in CASE_A_HV_HYBRID subcases (Table 2).

TABLE 3. Discharged BESSs location and other system features in subcases of CASE_A_HV_HYBRID (Fig. 4, Table 1).

Subcase	Location of BESSs
CASE A HV HYBRID Pf (U-FLL) ^{*)} , ^{**)}	Beginning of HV line
CASE A HV HYBRID Pf 2 (U-FLL) ^{*)} , ^{**)}	End of HV line
CASE A HV HYBRID Pf 2B (U-FLL) ^{*)} , ^{**)}	Middle of HV line
CASE A HV HYBRID Pf 2C (U-FLL) ^{*)} , ^{**)}	End of HV line

^{*)} HV line with series compensation (inductive reactance is reduced 25 %), ^{**)} Pf-control frequency input (Fig. 3) from PSCAD FFT –block with moving average over 100 ms, ^{**)} Pf-control frequency input has also moving average component over 100 ms after Pf-droop (Fig. 3)

TABLE 4. Discharged BESSs Pf-droop settings in subcases of CASE_A_HV_HYBRID (Fig. 4 and 16, Table 1).

Subcase	Pf-droop
CASE A HV HYBRID Pf (U-FLL) ^{*)} , ^{**)}	1
CASE A HV HYBRID Pf II (U-FLL) ^{*)} , ^{**)}	2
CASE A HV HYBRID Pf III (U-FLL) ^{*)} , ^{**)}	3
CASE A HV HYBRID Pf IV (U-FLL) ^{*)} , ^{**)}	4

^{*)} Pf-control frequency input (Fig. 3) from PSCAD FFT –block with moving average over 100 ms, ^{**)} Pf-control frequency input has also moving average component over 100 ms after Pf-droop

points of the network as well as with different measurement inputs and moving averages. These characteristics will also have an effect on Pf-droop-based active power control-dependent frequency support of BESSs. In addition, the worsening effect of larger Pf-control moving averaging i.e. 250 ms (Table 2) in CASE_A_HV_HYBRID_Pf_Qf instead of 100 ms (Table 2) in CASE_A_HV_HYBRID_Pf on active power support of BESSs (Fig. 12) and frequency support can be seen from Fig. 9-11.

2) A.2 BESSs LOCATION AND PF-CONTROL EFFECTIVENESS
 The simulation results from case CASE_A_HV_HYBRID (Fig. 4 and Table 1) subcases (Table 3) for studying the effect of BESSs' location in transmission network and addition of transmission line series compensation on frequency stability and Pf-control effectiveness are shown in Fig. 14 and 15. All BESSs in Table 3 subcases were controlled with Pf- and QU-droops (Fig. 8).

It can be seen from Fig. 14 that when the BESSs are at the end of HV line (i.e. closer to the increased load) in CASE_A_HV_HYBRID_Pf_2 (Table 3), the frequency stabil-

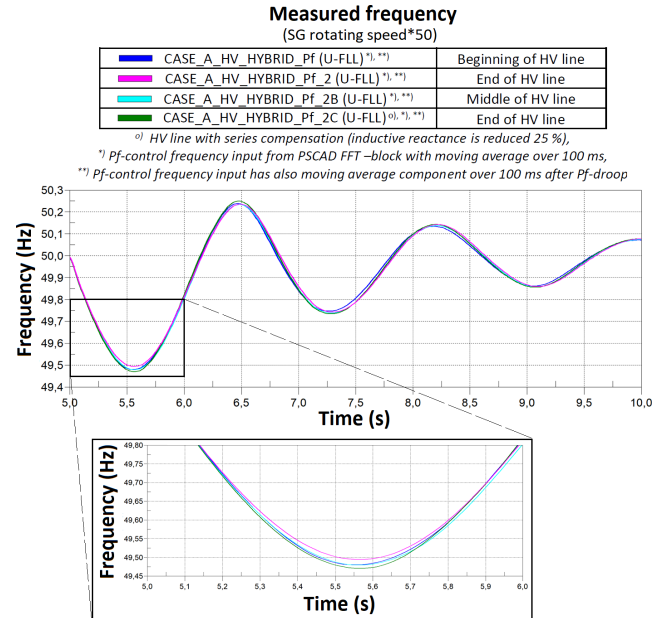


FIGURE 14. Measured frequency calculated from rotor speed of SG after load increase at $t = 5.0$ s with discharged BESSs in CASE_A_HV_HYBRID subcases (Table 3).

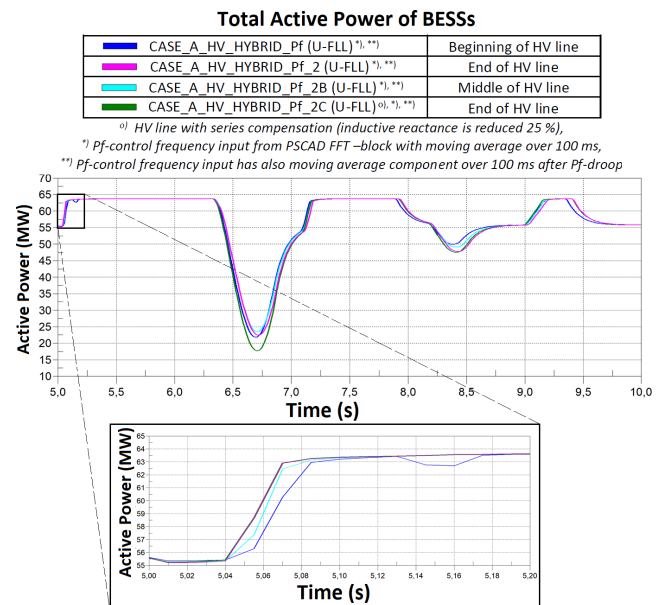


FIGURE 15. Total active power of all 16 BESSs after load increase at $t = 5.0$ s with discharged BESSs in CASE_A_HV_HYBRID subcases (Table 3).

ity is a bit improved. However, when series compensation is added to the HV line in CASE_A_HV_HYBRID_Pf_2C (Table 3) the first swing stability (Fig. 14) is even worse than in case CASE_A_HV_HYBRID_Pf (Table 3) with BESSs at the beginning of HV line, although total active power response of BESSs (Fig. 15) is better.

3) A.3 EFFECT OF PF-DROOP CONTROL PARAMETERS
 The simulation results from case CASE_A_HV_HYBRID (Fig. 4 and Table 1) subcases (Table 4) for studying the effect

of *Pf*-droop settings (Fig. 16) on frequency stability and *Pf*-control effectiveness are presented in Fig. 17 and 18.

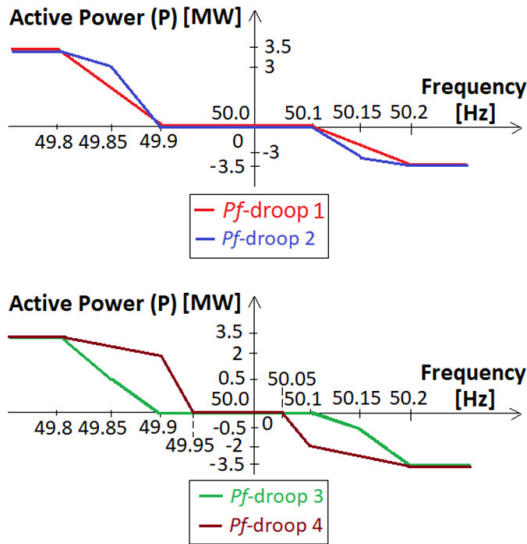


FIGURE 16. BESS's *Pf*-droop settings in Table 4 subcases.

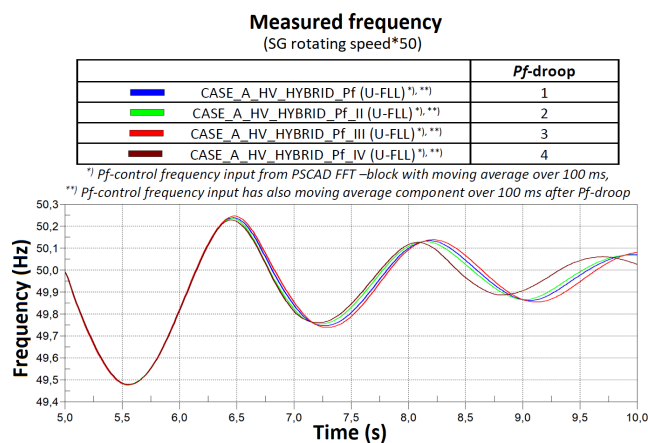


FIGURE 17. Measured frequency calculated from rotor speed of SG after load increase at $t = 5.0$ s with discharged BESSs in CASE_A_HV_HYBRID subcases (Table 4).

All BESSs in Table 4 subcases were controlled with *Pf*- and *QU*-droops (Fig. 8) and connected at the beginning of HV line (Fig. 4).

One can see from Fig. 16-18 that more sensitive *Pf*-droop settings in CASE_A_HV_HYBRID_Pf_IV (Table 4) have a positive effect on frequency stability after the load increase. Due to the delays in the frequency measurement (e.g. filtering and moving averaging related), the actual active power response of the *Pf*-droop controlled BESS unit is not as rapid as possible. Therefore, frequency stability support of BESSs could be improved if this delayed response is compensated by using more sensitive *Pf*-droop settings than those that are actually required nowadays by frequency control market or grid code requirements. In the future, the *Pf*-droop settings could possibly be adaptive also so that they would take into

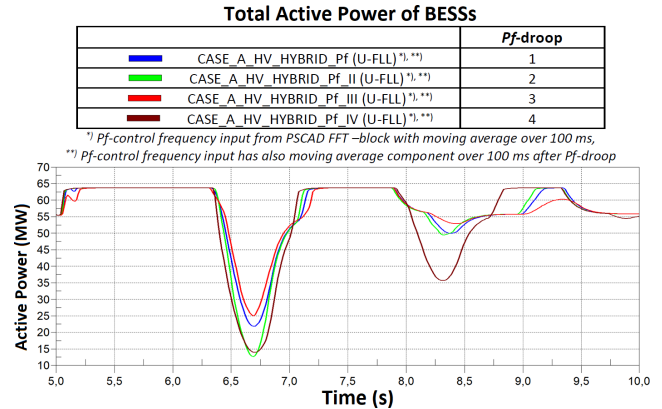


FIGURE 18. Total active power of all 16 BESSs after load increase at $t = 5.0$ s with discharged BESSs in CASE_A_HV_HYBRID subcases (Table 4).

account the monitored and forecasted power system inertia level.

B. SMALL HYBRID HV NETWORK – CHARGING OF BESSs

Total simulation time in Section IV-B subcases was $t = 20.0$ s and 100 MW load increase at the end of 50 km transmission line (Fig. 4) happened at $t = 5.0$ s. Before the load increase in Section IV-B subcases the total load was 450.5 MW and total active power load of 16 charged BESSs was 56 MW. BESS mode change from charging to discharging during frequency oscillations would have improved the frequency stability support, but operation mode change was disabled in the simulations of Section IV-B.

TABLE 5. Charged BESSs control scheme differences in subcases of CASE_B_HV_HYBRID_loads (Fig. 4, Table 1).

Subcase	Location of BESSs	BESS control
CASE_B_HV_HYBRID_loads (U-FLL)	Beginning of HV line	No <i>Pf</i> -control, <i>QU</i> -control
CASE_B_HV_HYBRID_loads_Pf (U-FLL) ^{*)}	Beginning of HV line	<i>Pf</i> -control, <i>QU</i> -control
CASE_B_HV_HYBRID_loads_Pf_2 (U-FLL) ^{*)}	End of HV line	<i>Pf</i> -control, <i>QU</i> -control

^{*)} *Pf*-control frequency input (Fig. 3) from PSCAD FFT-block with moving average over 100 ms, ^{**)} *Pf*-control frequency input has also moving average component over 100 ms after *Pf*-droop

1) B.1 EFFECT OF CHARGED BESSs PF-CONTROL

The simulation results from case CASE_B_HV_HYBRID_loads (Fig. 4 and Table 1) subcases (Table 5) for studying the effect of charged BESSs' *Pf*-control with *Pf*-droop 1 (Fig. 16) are shown in Fig. 19 and 20.

Fig. 19 shows the positive effect of charged BESSs' *Pf*-droop control on frequency stability in CASE_B_HV_HYBRID_loads_Pf when compared to case without it in CASE_B_HV_HYBRID_loads. Fig. 19 presents also the advantages when *Pf*-controlled BESSs are at the end of HV line closer to the increased load in CASE_B_HV_HYBRID_loads_Pf_2

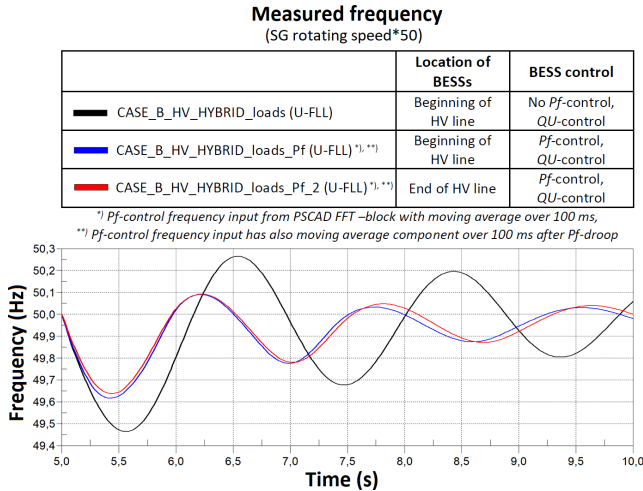


FIGURE 19. Measured frequency calculated from rotor speed of SG after load increase at $t = 5.0$ s with charged BESSs in CASE_B_HV_HYBRID_loads subcases (Table 5).

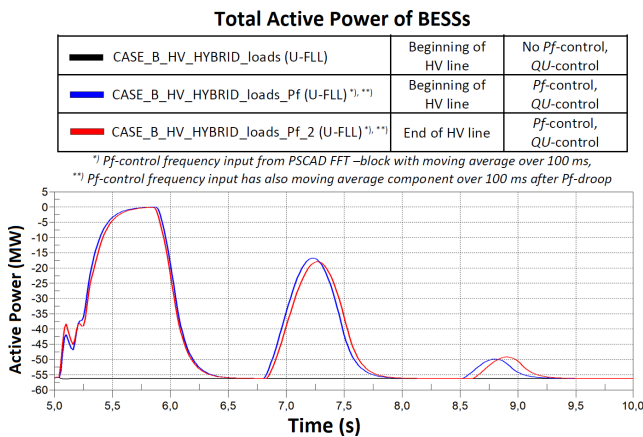


FIGURE 20. Total active power of all 16 BESSs after load increase at $t = 5.0$ s with charged BESSs in CASE_B_HV_HYBRID_loads subcases (Table 5).

(Table 5). In addition, during charging of BESSs (operation as loads) the positive effect of Pf-control was even more significant (Fig. 19) when compared to pure discharged operation of BESSs (operation only as generation) in Fig. 9 due to larger amount of controllable active power during first swing after load connection.

2) B.2 EFFECT OF INPUT FREQUENCY ON CHARGED BESSs PF-CONTROL

The simulation results from case CASE_B_HV_HYBRID_loads_Pf (Fig. 4 and Table 1) subcases (Table 6) for studying the effect of Pf-control’s input frequency and input modification of U-FLL on charged BESSs with Pf-droop 1 (Fig. 16) are shown in Fig. 22 and 23. In these subcases (Table 6) all 16 BESS were connected closer to the beginning of HV line and were using QU-control.

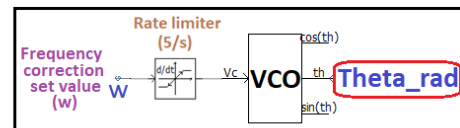
From Fig. 22 the positive effect of rate limiter (3/s) on BESSs’ Pf-droop control on frequency stability can be seen

TABLE 6. Charged BESSs differences in input frequency of Pf-control and input of U-FLL in subcases of CASE_B_HV_HYBRID_loads_Pf (Fig. 3, 4 and 21, Table 1).

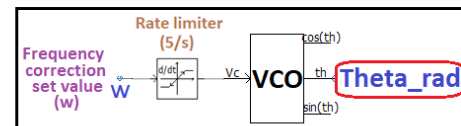
Subcase	U-FLL input	Pf-control input ^{*)}
CASE_B_HV_HYBRID_loads_Pf (U-FLL)	No modification ⁾	No modification ^{**)}
CASE_B_HV_HYBRID_loads_Pf_rate (U-FLL)	Rate limiter (5/s) ⁾	No modification ^{**)}
CASE_B_HV_HYBRID_loads_Pf_rate2 (U-FLL)	Rate limiter (5/s) ⁾	Rate limiter (3/s) ^{**)}
CASE_B_HV_HYBRID_loads_Pf_freq (U-FLL)	Frequency from PSCAD measurement block ^{o)}	Frequency from PSCAD measurement block ^{o)}

⁾ U-FLL frequency input (Fig. 3) from PSCAD FFT-block with moving average over 5 ms, ^{**)} Pf-control frequency input (Fig. 3) from PSCAD FFT-block with moving average over 100 ms, ^{o)} Pf-control frequency input has also moving average component over 100 ms after Pf-droop (Fig. 3), ^{o)} PSCAD frequency measurement block (Fig. 21) has 20 ms washout constant for phase measurement

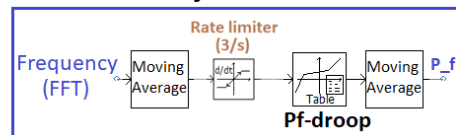
CASE_B_HV_HYBRID_loads_Pf_rate (U-FLL)



CASE_B_HV_HYBRID_loads_Pf_rate2 (U-FLL)



Pf-control



CASE_B_HV_HYBRID_loads_Pf_freq (U-FLL)

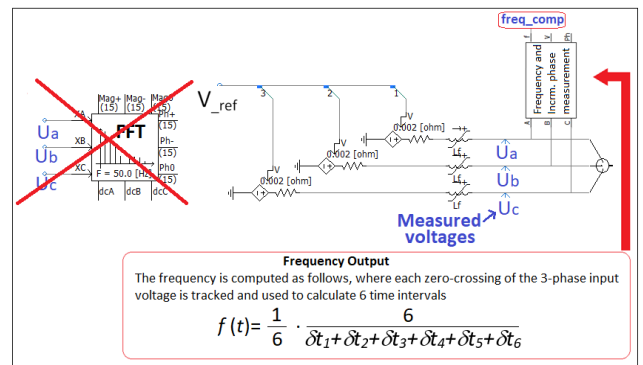


FIGURE 21. Charged BESSs differences in input frequency of Pf-control and input of U-FLL in subcases of CASE_B_HV_HYBRID_loads_Pf (Table 6).

in CASE_B_HV_HYBRID_loads_Pf_rate2 (Table 6) when compared to case without it i.e. CASE_B_HV_HYBRID_loads_Pf (Table 6). In addition, it can be seen from Fig. 22 and 23 how 20 ms washout constant in CASE_B_HV_HYBRID_loads_Pf_freq (Fig. 21, Table 6) instead of 100 ms moving average

Measured frequency
(SG rotating speed*50)

	U-FLL input	Pf-control input ^(**)
CASE_B_HV_HYBRID_loads_Pf (U-FLL)	No modification ^(*)	No modification ^(**)
CASE_B_HV_HYBRID_loads_Pf_rate (U-FLL)	Rate limiter (5/s) ^(*)	No modification ^(**)
CASE_B_HV_HYBRID_loads_Pf_rate2 (U-FLL)	Rate limiter (5/s) ^(*)	Rate limiter (3/s) ^(**)
CASE_B_HV_HYBRID_loads_Pf_freq (U-FLL)	Frequency from PSCAD measurement block ^(*)	Frequency from PSCAD measurement block ^(*)

^(*) U-FLL frequency input from PSCAD FFT –block with moving average over 5 ms,
^(**) Pf-control frequency input from PSCAD FFT –block with moving average over 100 ms,
^(***) Pf-control frequency input has also moving average component over 100 ms after Pf-droop,
^(*) PSCAD frequency measurement block has 20 ms washout constant for phase measurement

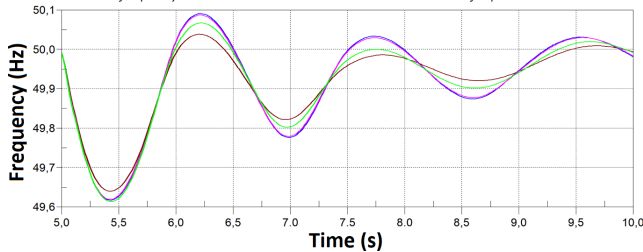


FIGURE 22. Measured frequency calculated from rotor speed of SG after load increase at $t = 5.0$ s with charged BESSs in CASE_B_HV_HYBRID_loads_Pf subcases (Table 6).

Total Active Power of BESSs

	U-FLL input	Pf-control input ^(**)
CASE_B_HV_HYBRID_loads_Pf (U-FLL)	No modification ^(*)	No modification ^(**)
CASE_B_HV_HYBRID_loads_Pf_rate (U-FLL)	Rate limiter (5/s) ^(*)	No modification ^(**)
CASE_B_HV_HYBRID_loads_Pf_rate2 (U-FLL)	Rate limiter (5/s) ^(*)	Rate limiter (3/s) ^(**)
CASE_B_HV_HYBRID_loads_Pf_freq (U-FLL)	Frequency from PSCAD measurement block ^(*)	Frequency from PSCAD measurement block ^(*)

^(*) U-FLL frequency input from PSCAD FFT –block with moving average over 5 ms,
^(**) Pf-control frequency input from PSCAD FFT –block with moving average over 100 ms,
^(***) Pf-control frequency input has also moving average component over 100 ms after Pf-droop,
^(*) PSCAD frequency measurement block has 20 ms washout constant for phase measurement

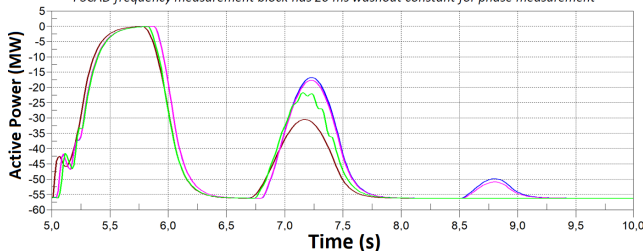


FIGURE 23. Total active power of all 16 BESSs after load increase at $t = 5.0$ s with charged BESSs in CASE_B_HV_HYBRID_loads_Pf subcases (Table 6).

with BESSs’ frequency input in Pf-droop control enables faster active power response and better frequency stability support.

C. SMALL HYBRID HV NETWORK – TWO BESSs AT THE CONNECTION POINT OF SG

1) C.1 EFFECT OF DIFFERENT INPUT FREQUENCIES ON PF-CONTROL OF BESS

The simulation results from subcases (Table 7) with two additional 4 MW BESSs at the SG connection point (Fig. 5) are shown in Fig. 25 and 26. In the subcases the effect of these two BESSs’ Pf-control input frequency and input

TABLE 7. Two additional discharged/charged BESSs differences in input frequency of Pf-control and input of U-FLL in subcases of CASE_C_HV_HYBRID (Fig. 3, 5 and 24, Table 1).

Subcase	U-FLL input	Pf-control input ^(***)
CASE_C_HV_HYBRID_Pf_BESS (U-FLL)	No modification ^(*)	No modification ^(**)
CASE_C_HV_HYBRID_Pf_BESS_1 (U-FLL)	Delay compensation ^(*)	No modification ^(**)
CASE_C_HV_HYBRID_Pf_BESS_2 (U-FLL)	No modification ^(*)	Frequency input from SG speed ^(**)
CASE_C_HV_HYBRID_Pf_BESS_3 (U-FLL)	Frequency input from SG speed ^(*)	Frequency input from SG speed ^(**)

^(*) U-FLL frequency input (Fig. 3) from PSCAD FFT –block or SG rotating speed with moving average over 5 ms, ^(**) Pf-control frequency input (Fig. 3) from PSCAD FFT –block with moving average over 100 ms, ^(***) Pf-control frequency input has also moving average component over 100 ms after Pf-droop (Fig. 3), ^(*) U-FLL frequency input (Fig. 3) from PSCAD FFT –block with moving average over 50 ms, ^(**) U-FLL frequency input (Fig. 3) from SG speed without moving averaging

modification of U-FLL (Fig. 24) on frequency stability during discharged/charged operation with Pf-droop 1 (Fig. 16) is studied. BESS mode change from charging to discharging during frequency oscillations was enabled in the simulations of Section IV-C. The studied changes in input frequency of Pf-droop control and input of U-FLL are different in this Section IV-C1 than in previous Section IV-B2.

Initial active power output of the two BESSs at the SG connection point was close to zero before the load increase. Total simulation time in Table 7 subcases was $t = 20.0$ s and 100 MW load increase at the end of 50 km transmission line (Fig. 5) happened at $t = 5.0$ s. Before the load increase the total load was 505.5 MW and total active power generation of 16 discharged BESSs was 56 MW. In addition, in these subcases (Table 7) all 16 BESS were connected at the beginning of HV line and were using QU-control.

It can be seen from Fig. 25, for instance, that the delay compensation in CASE_C_HV_HYBRID_Pf_BESS_1 (Fig. 24, Table 7), which is used in U-FLL input, has positive effect on frequency stability only after $t = 10.0$ s (i.e. 5 s after the load increase, Fig. 25) when compared to CASE_C_HV_HYBRID_Pf_BESS without any modification (Table 7). In addition, it can be seen from Fig. 25 and 26 that the best frequency stability support from these two additional BESSs at SG connection point can be achieved in CASE_C_HV_HYBRID_Pf_BESS_2 (Table 7) and CASE_C_HV_HYBRID_Pf_BESS_3 (Table 7) where SG’s rotor rotating speed is used as an input for Pf-control. In CASE_C_HV_HYBRID_Pf_BESS_3 (Table 7) SG’s rotor speed is also used as input for U-FLL (Fig. 24).

2) C.2 EFFECT OF COMMUNICATION TIME DELAY ON PF-CONTROL OF BESS

The simulation results from subcases (Table 8) with two additional 4 MW BESSs at the SG connection point (Fig. 5) are presented in Fig. 28 and 29. In these subcases the effect of frequency measurement’s 50 or 200 ms communication delay (Fig. 27) on Pf-control effectiveness and frequency

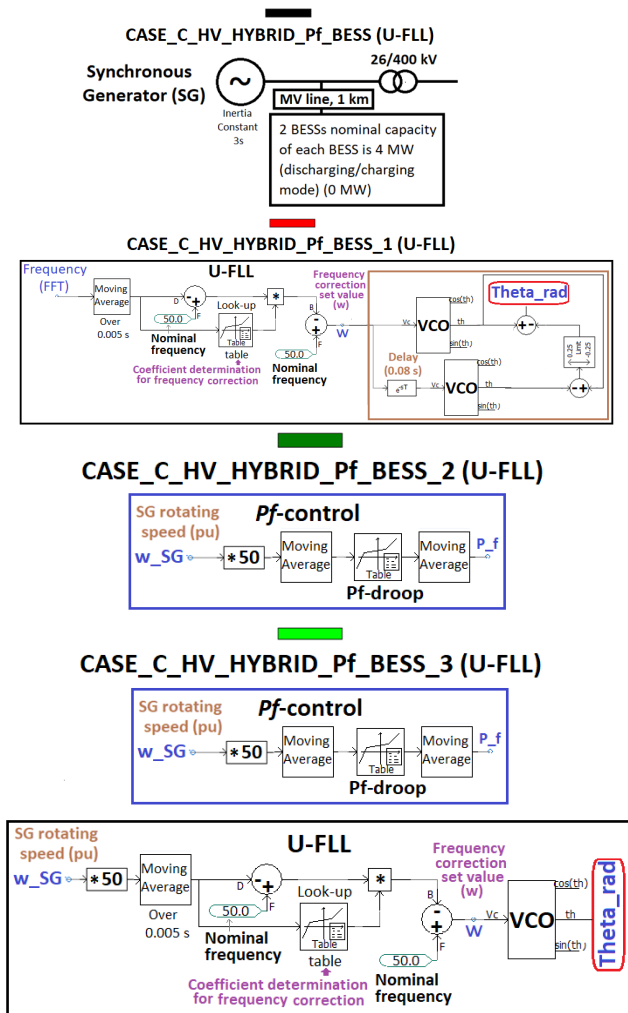


FIGURE 24. Two additional charged/charged BESSs at the connection point of SG and their differences in input frequency of Pf-control and input of U-FLL in subcases of CASE_C_HV_HYBRID (Table 7).

TABLE 8. Two additional discharged/charged BESSs differences in input frequency of Pf-control and input of U-FLL in subcases of CASE_C_HV_HYBRID_Pf_BESS_3 (Fig. 3, 5 and 27, Table 1).

Subcase	U-FLL input	Pf-control input ^{*)}
CASE_C_HV_HYBRID_Pf_BESS_3 (U-FLL)	Frequency input from SG speed ^{*)}	Frequency input from SG speed ^{o)}
CASE_C_HV_HYBRID_Pf_BESS_3_50ms (U-FLL)	50 ms delayed frequency input from SG speed ^{*)}	50 ms delayed frequency input from SG speed ^{o)}
CASE_C_HV_HYBRID_Pf_BESS_3_200ms (U-FLL)	200 ms delayed frequency input from SG speed ^{*)}	200 ms delayed frequency input from SG speed ^{o)}

^{*)} U-FLL frequency input (Fig. 3) from PSCAD FFT-block or SG rotating speed with moving average over 5 ms, ^{**)} Pf-control frequency input has also moving average component over 100 ms after Pf-droop (Fig. 3), ^{o)} U-FLL frequency input (Fig. 3) from SG speed without moving averaging

stability is studied. The main characteristics of these subcases (Table 8) are similar in this Section IV-C2 than in the previous Section IV-C1.

Measured frequency (SG rotating speed*50)

	U-FLL input	Pf-control input ^{*)}
CASE_A_HV_HYBRID_Pf (U-FLL) (WITHOUT TWO BESSs AT THE CONNECTION POINT OF SG)	No modification ^{*)}	No modification ^{*)}
CASE_C_HV_HYBRID_Pf_BESS (U-FLL)	No modification ^{*)}	No modification ^{*)}
CASE_C_HV_HYBRID_Pf_BESS_1 (U-FLL)	Delay compensation ^{o)}	No modification ^{*)}
CASE_C_HV_HYBRID_Pf_BESS_2 (U-FLL)	No modification ^{*)}	Frequency input from SG speed ^{o)}
CASE_C_HV_HYBRID_Pf_BESS_3 (U-FLL)	Frequency input from SG speed ^{*)}	Frequency input from SG speed ^{o)}

^{*)} U-FLL frequency input from PSCAD FFT-block or SG rotating speed with moving average over 5 ms, ^{**)} Pf-control frequency input from PSCAD FFT-block with moving average over 100 ms, ^{***)} Pf-control frequency input has also moving average component over 100 ms after Pf-droop, ^{o)} U-FLL frequency input from PSCAD FFT-block with moving average over 50 ms, ^{oo)} U-FLL frequency input from SG speed without moving averaging

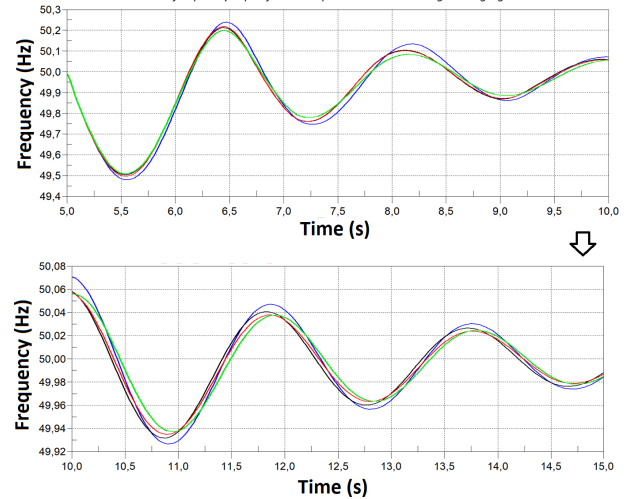


FIGURE 25. Measured frequency calculated from rotor speed of SG after load increase at $t = 5.0$ s with two additional BESSs at the connection point of SG in CASE_C_HV_HYBRID subcases (Table 7).

Fig. 28 shows that 50 ms communication time delay in frequency measurement which is calculated from the SG rotor speed in CASE_C_HV_HYBRID_Pf_BESS_3_50ms (Fig. 27, Table 8) does not have very notable effect on frequency stability after load increase. However, longer 200 ms communication time delay (CASE_C_HV_HYBRID_Pf_BESS_3_200ms) already has notable negative effect on frequency stability (Fig. 28). On the other hand, for example, GPS- [34], GNSS- or IEEE 1588 Precision Time Protocol (PTP)-based (e.g. in 5G networks) time synchronization could compensate communication time delays related issues.

D. SMALL HV NETWORK WITH 100 % IBR-BASED GENERATION

In the following, the simulation results with 100 % IBR-based generation (68 BESSs, Fig. 3 and 6, Table 1) in CASE_HV_IBR are shown. It was concluded in [10] that the U-FLL-based synchronization can enable stable frequency, also after load increase, in 100 % IBR-based small HV network with 68 BESSs connected in MV network many kilometers away from each other (Fig. 6).

Nominal capacity of each BESS is 4 MW. Total generation of the BESSs' is 230 MW consisting of 64 BESSs with

Total Active Power of two BESSs	U-FLL input	Pf-control input ^(*)
CASE_C_HV_HYBRID_Pf_BESS (U-FLL)	No modification ^(*)	No modification ^(*)
CASE_C_HV_HYBRID_Pf_BESS_1 (U-FLL)	Delay compensation ^(*)	No modification ^(*)
CASE_C_HV_HYBRID_Pf_BESS_2 (U-FLL)	No modification ^(*)	Frequency input from SG speed ^(*)
CASE_C_HV_HYBRID_Pf_BESS_3 (U-FLL)	Frequency input from SG speed ^(*)	Frequency input from SG speed ^(*)

^(*) U-FLL frequency input from PSCAD FFT-block or SG rotating speed with moving average over 5 ms, ^(**) Pf-control frequency input from PSCAD FFT-block with moving average over 100 ms, ^(***) Pf-control frequency input has also moving average component over 100 ms after Pf-droop, ^(****) U-FLL frequency input from PSCAD FFT-block with moving average over 50 ms, ^(o) U-FLL frequency input from SG speed without moving averaging

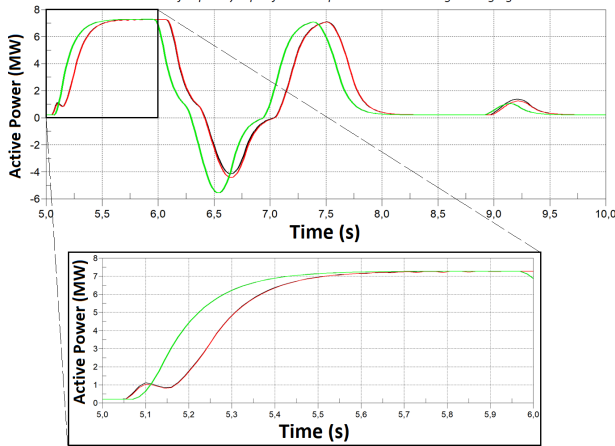


FIGURE 26. Total active power of two additional BESSs after load increase at $t = 5.0$ s with two additional BESSs at the connection point of SG in CASE_C_HV_HYBRID subcases (Table 7).

CASE_C_HV_HYBRID_Pf_BESS_3_50ms (U-FLL)
 CASE_C_HV_HYBRID_Pf_BESS_3_200ms (U-FLL)

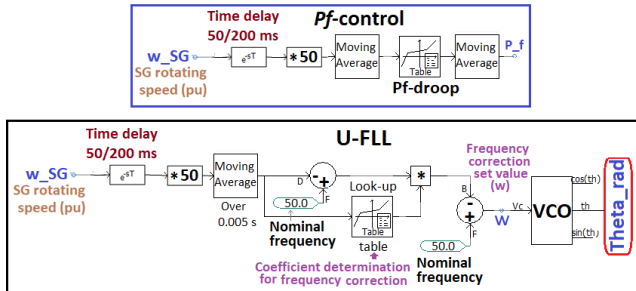


FIGURE 27. Two additional charged/charged BESSs at the connection point of SG with 50 or 200 ms delayed frequency measurement used as input for Pf-control and U-FLL in subcases of CASE_C_HV_HYBRID_Pf_BESS_3 (Table 8).

3.5 MW generation (224 MW) and 4 BESSs with 1.5 MW generation (6 MW). These 4 BESS also act as reactive power “slack bus” during 100 % IBR operation i.e. reactive power Q reference input is 0. In 100 % IBR-based system Pf-control is not applicable with the used control schemes and therefore PU -control and Q -control are used with BESSs (Fig. 3). Total load at the end of 50 HV transmission line is 225 MW. During the 25.0 s simulation load increases at the end of 50 km HV transmission line at $t = 15.0$ s 15 MW.

Measured frequency (SG rotating speed*50)	U-FLL input	Pf-control input ^(*)
CASE_C_HV_HYBRID_Pf_BESS_3 (U-FLL)	Frequency input from SG speed ^(*)	Frequency input from SG speed ^(*)
CASE_C_HV_HYBRID_Pf_BESS_3_50ms (U-FLL)	50 ms delayed frequency input from SG speed ^(*)	50 ms delayed frequency input from SG speed ^(*)
CASE_C_HV_HYBRID_Pf_BESS_3_200ms (U-FLL)	200 ms delayed frequency input from SG speed ^(*)	200 ms delayed frequency input from SG speed ^(*)

^(*) U-FLL frequency input from PSCAD FFT-block or SG rotating speed with moving average over 5 ms, ^(**) Pf-control frequency input has also moving average component over 100 ms after Pf-droop, ^(o) U-FLL frequency input from SG speed without moving averaging

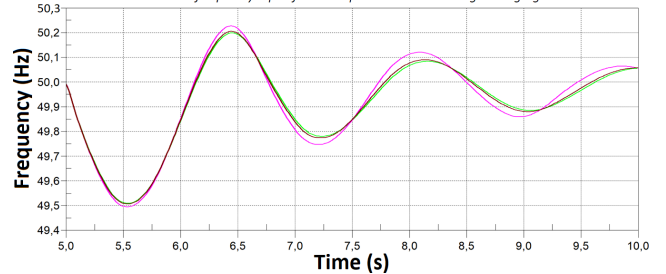


FIGURE 28. Measured frequency calculated from rotor speed of SG after load increase at $t = 5.0$ s with two additional BESSs at the connection point of SG in CASE_C_HV_HYBRID_Pf_BESS_3 subcases (Table 8).

Total Active Power of two BESSs	U-FLL input	Pf-control input ^(*)
CASE_C_HV_HYBRID_Pf_BESS_3 (U-FLL)	Frequency input from SG speed ^(*)	Frequency input from SG speed ^(*)
CASE_C_HV_HYBRID_Pf_BESS_3_50ms (U-FLL)	50 ms delayed frequency input from SG speed ^(*)	50 ms delayed frequency input from SG speed ^(*)
CASE_C_HV_HYBRID_Pf_BESS_3_200ms (U-FLL)	200 ms delayed frequency input from SG speed ^(*)	200 ms delayed frequency input from SG speed ^(*)

^(*) U-FLL frequency input from PSCAD FFT-block or SG rotating speed with moving average over 5 ms, ^(**) Pf-control frequency input has also moving average component over 100 ms after Pf-droop, ^(o) U-FLL frequency input from SG speed without moving averaging

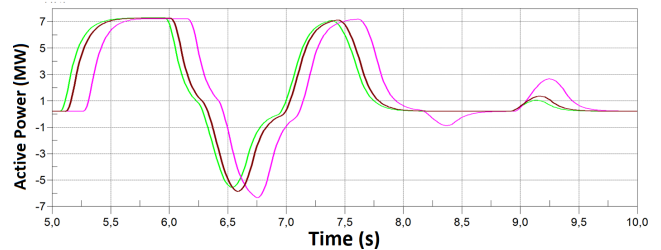


FIGURE 29. Total active power of two additional BESSs after load increase at $t = 5.0$ s with two additional BESSs at the connection point of SG in CASE_C_HV_HYBRID_Pf_BESS_3 subcases (Table 8).

1) D.1 EFFECT OF MODIFIED U-FLL

The simulation results from case CASE_HV_IBR (Fig. 6 and Table 1) subcases (Table 9) for studying the effect of modified U-FLL (Fig. 30) on frequency behavior and stability after load increase are shown in Fig. 31.

It can be seen from Fig. 31 that modified adaptive (frequency-dependent) coefficient can enable smaller frequency change after disturbance in CASE_HV_IBR_B and

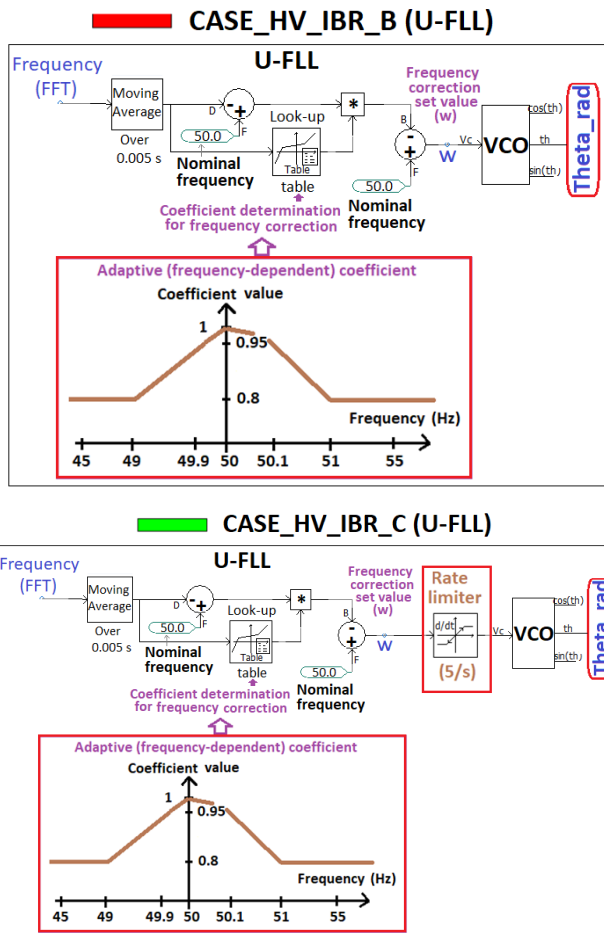


FIGURE 30. U-FLL modifications in BESS control scheme (Fig. 3) in subcases of CASE_HV_IBR (Table 9).

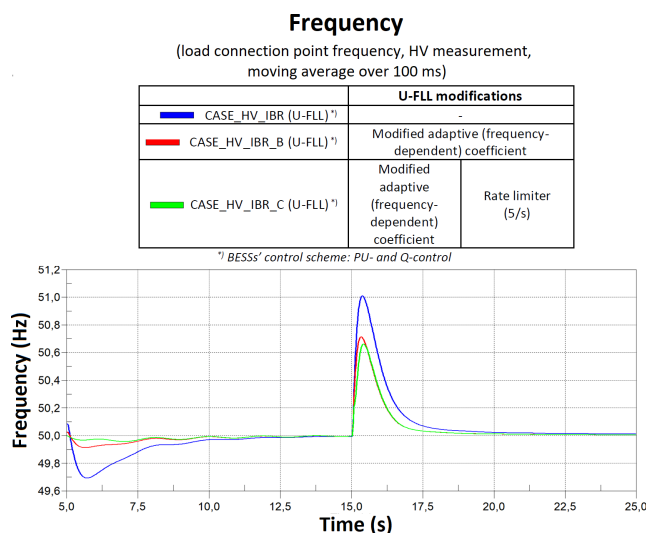


FIGURE 31. Measured frequency (load connection point frequency, HV measurement, moving average over 100 ms, Fig. 6) after load increase at $t = 15.0$ s in CASE_HV_IBR subcases (Table 9).

CASE_HV_IBR_C (Fig. 30 and Table 9). Fig. 31 also shows that utilization of rate limiter (5/s) in U-FLL (CASE_HV_IBR_C, Fig. 30), in addition to modified adaptive

TABLE 9. U-FLL modifications in BESS control scheme in subcases of CASE_HV_IBR (Fig. 3, 6 and 30, Table 1).

Subcase	U-FLL modifications	
CASE_HV_IBR (U-FLL) ^{*)}	-	
CASE_HV_IBR_B (U-FLL) ^{*)}	Modified adaptive (frequency-dependent) coefficient	
CASE_HV_IBR_C (U-FLL) ^{*)}	Modified adaptive (frequency-dependent) coefficient	Rate limiter (5/s)

^{*)} BESSs' control scheme: PU- and Q-control (Fig. 3)

coefficient, can further improve the frequency stabilization after the load increase.

V. CONCLUSION

Future power systems with IBRs will have different dynamics due to lack of natural kinetic inertia from large rotating SGs. In addition, the frequency stability of future low-inertia power systems will be determined increasingly by the control schemes of IBRs, their stability and other characteristics. The effect increases when the share of IBRs with GFL and GFM control methods is high compared to the SGs. In this paper, the grid-forming and supporting universal U-FLL-based control and grid synchronization for IBR-based BESSs was utilized to improve the frequency stability of a simple power system i.e. small HV network. Multiple PSCAD simulation studies were performed and based on the simulations following general conclusions were made for hybrid power system (including SG and BESSs):

- *Pf*-control of BESS is beneficial for frequency stability after large disturbance (e.g. major load increase), but processing of frequency measurement e.g. with moving averaging can delay the active power response and frequency stability support of the BESS,
- More sensitive (than required e.g. in grid code or frequency market requirements) or adaptive *Pf*-droop settings of BESS could enable improved frequency stability support and compensation of delays in the frequency measurement (e.g. due to filtering and moving averaging of measured signals),
- Utilization of rate limiter (3/s) on BESSs' *Pf*-droop control can improve frequency stability support and enable faster active power provision of BESS after disturbance,
- During charging of BESSs (operation only as loads i.e. change of operation mode during frequency oscillations was disabled) the positive effect of *Pf*-control was even more significant when compared to discharged operation of BESSs (operation as generation i.e. change of operation mode during frequency oscillations was disabled) due to larger amount of controllable active power during first swing after load connection (dependent on the active power output before disturbance/event),
- *Pf*-controlled discharged and charged BESSs close to the disturbance (e.g. load increase) can provide better frequency stability support than BESSs further away,

- HV line series compensation can decrease frequency stability and
- BESS at the connection point of SG can improve the frequency stability after disturbance with operation mode change from discharged to charged enabled during frequency oscillations and also especially if SG rotor speed is used as an input for frequency measurement which is utilized in P_f -control of BESS and the communication time delay is less than 50 ms.

In addition, in simulations with 100 % IBR-based small HV network (with 68 distributed BESSs) two different U-FLL modifications were studied. Based on these simulations the utilization of modified adaptive (frequency-dependent) coefficient and rate limiter (5/s) could enable smaller frequency change after disturbance (e.g. load increase).

In the future works, the potential advantages of studied and developed features like, for example, related to the functionality of the P_f -controlled and U-FLL-based BESS which utilizes SG rotating speed as frequency measurement input and the possibility of compensating communication time delay related issues, for example, in 5G networks with IEEE 1588 PTP-based time synchronization could be further studied and verified with laboratory testing before real-life experiments.

REFERENCES

- [1] A. Tuohy, P. Dattaray, E. Farantatos, A. Kelly, and E. Lannoye, "Implications of reduced inertia levels on the electricity system: Technical report on the challenges and solutions for system operations with very high penetrations of non-synchronous resources," EPRI, Palo Alto, CA, USA, Tech. Rep. 3002014970, 2019. [Online]. Available: <https://www.epri.com/research/products/000000003002014970>
- [2] P. Denholm, T. Mai, R. W. Kenyon, B. Kroposki, and M. O'Malley, "Inertia and the power grid: A guide without the spin," Nat. Renew. Energy Lab., Golden, CO, USA, Tech. Rep. NREL/TP-6120-73856, 2020. [Online]. Available: <https://www.nrel.gov/docs/fy20osti/73856.pdf>
- [3] O. Lehtinen and A. Alahäivälä. (2022). *Towards Stable and Reliable 100% Renewable Energy Grids—White Paper on Power System Stability*. Wärtsilä. [Online]. Available: <https://cdn.wartsila.com/docs/default-source/power-plants-documents/downloads/white-papers/general/towards-stable-and-reliable-100-renewable-energy-grids.pdf>
- [4] F. Milano, F. Dorfler, G. Hug, D. J. Hill, and G. Verbic, "Foundations and challenges of low-inertia systems (invited paper)," in *Proc. Power Syst. Comput. Conf. (PSCC)*, Jun. 2018, pp. 1–25, doi: [10.23919/PSCC.2018.8450880](https://doi.org/10.23919/PSCC.2018.8450880).
- [5] R. Rosso, X. Wang, M. Liserre, X. Lu, and S. Engelken, "Grid-forming converters: Control approaches, grid-synchronization, and future trends—A review," *IEEE Open J. Ind. Appl.*, vol. 2, pp. 93–109, 2021, doi: [10.1109/OJIA.2021.3074028](https://doi.org/10.1109/OJIA.2021.3074028).
- [6] J. Rocabert, A. Luna, F. Blaabjerg, and P. Rodriguez, "Control of power converters in AC microgrids," *IEEE Trans. Power Electron.*, vol. 27, no. 11, pp. 4734–4749, Nov. 2012.
- [7] X. Wang, M. G. Taul, H. Wu, Y. Liao, F. Blaabjerg, and L. Harnefors, "Grid-synchronization stability of converter-based resources—An overview," *IEEE Open J. Ind. Appl.*, vol. 1, pp. 115–134, 2020, doi: [10.1109/OJIA.2020.3020392](https://doi.org/10.1109/OJIA.2020.3020392).
- [8] L. Zhang, L. Harnefors, and H. P. Nee, "Power-synchronization control of grid-connected voltage-source converters," *IEEE Trans. Power Syst.*, vol. 25, no. 2, pp. 809–820, Nov. 2010.
- [9] P. Unruh, M. Nuschke, P. Straub, and F. Welck, "Overview on grid-forming inverter control methods," *Energies*, vol. 13, no. 10, p. 2589, May 2020, doi: [10.3390/en13102589](https://doi.org/10.3390/en13102589).
- [10] H. Laaksonen, "Universal grid-forming method for future power systems," *IEEE Access*, vol. 10, pp. 133109–133125, 2022, doi: [10.1109/ACCESS.2022.3231479](https://doi.org/10.1109/ACCESS.2022.3231479).
- [11] N. Modig, R. Eriksson, P. Ruokolainen, J. N. Ødegård, S. Weizenegger, and T. D. Fechtenburg. (2022). *Overview of Frequency Control in the Nordic Power System*. ENTSO-E. [Online]. Available: <https://www.eprints.com/media/userfiles/107305/1648196866/overview-of-frequency-control-in-the-nordic-power-system-1.pdf>
- [12] H. Yin, Y. Wu, W. Qiu, C. Zeng, S. You, J. Tan, A. Hoke, C. J. Kruse, B. W. Rockwell, K. A. Kawamura, and Y. Liu, "Precise ROCOF estimation algorithm for low inertia power grids," *Electric Power Syst. Res.*, vol. 209, Aug. 2022, Art. no. 107968, doi: [10.1016/j.epsr.2022.107968](https://doi.org/10.1016/j.epsr.2022.107968).
- [13] Y. Wang, Y. Xu, Y. Tang, K. Liao, M. H. Syed, E. Guillo-Sansano, and G. M. Burt, "Aggregated energy storage for power system frequency control: A finite-time consensus approach," *IEEE Trans. Smart Grid*, vol. 10, no. 4, pp. 3675–3686, Jul. 2019.
- [14] J. Vasilj, S. Gros, D. Jakus, and P. Sarajcev, "Multi-market scheduling of battery storages within renewable portfolios," in *Proc. IEEE PES Innov. Smart Grid Technol. Conf. Eur. (ISGT-Europe)*, Oct. 2018, pp. 21–25.
- [15] H. Laaksonen, C. Parthasarathy, H. Hafezi, M. Shafie-khah, H. Khajeh, and N. Hatziaegyriou, "Solutions to increase PV hosting capacity and provision of services from flexible energy resources," *Appl. Sci.*, vol. 10, no. 15, p. 5146, Jul. 2020, doi: [10.3390/app10155146](https://doi.org/10.3390/app10155146).
- [16] M. G. Dozein, "System dynamics of low-carbon grids: Fundamentals, challenges, and mitigation solutions," Ph.D. thesis, Dept. Elect. Electron. Eng., Univ. Melbourne, Melbourne, VIC, Australia, 2021.
- [17] P. Kundur, J. Paserba, V. Ajjarapu, G. Andersson, A. Bose, C. Canizares, N. Hatziaegyriou, D. Hill, C. Taylor, T. Van Cutsem, A. Stankovic, and V. Vittal, "Definition and classification of power system stability IEEE/CIGRE joint task force on stability terms and definitions," *IEEE Trans. Power Syst.*, vol. 19, no. 2, pp. 1387–1401, Aug. 2004.
- [18] N. Hatziaegyriou, J. Milanovic, C. Rahmann, V. Ajjarapu, C. Canizares, I. Erlich, D. Hill, I. Hiskens, I. Kamwa, B. Pal, P. Pourbeik, J. Sanchez-Gasca, A. Stankovic, T. Van Cutsem, V. Vittal, and C. Vournas, "Definition and classification of power system stability—revisited & extended," *IEEE Trans. Power Syst.*, vol. 36, no. 4, pp. 3271–3281, Jul. 2021, doi: [10.1109/TPWRS.2020.3041774](https://doi.org/10.1109/TPWRS.2020.3041774).
- [19] A. Hoke and V. Gevorgian, "Thoughts and hypotheses on the metrics and needs for the stability of highly inverter-based island systems [viewpoint]," *IEEE Electrific. Mag.*, vol. 10, no. 3, pp. 94–98, Sep. 2022, doi: [10.1109/MELE.2022.3187905](https://doi.org/10.1109/MELE.2022.3187905).
- [20] A. Crivellaro, A. Tayyebi, C. Gavriluta, D. Gross, A. Anta, F. Kupzog, and F. Dorfler, "Beyond low-inertia systems: Massive integration of grid-forming power converters in transmission grids," in *Proc. IEEE Power Energy Soc. Gen. Meeting (PESGM)*, Aug. 2020, pp. 1–5, doi: [10.1109/PESGM41954.2020.9282031](https://doi.org/10.1109/PESGM41954.2020.9282031).
- [21] Fingrid. (2020). *Subsynchronous Oscillation Risks of Wind Power Plants Connecting to Finnish Series Compensated Network*. [Online]. Available: <https://www.fingrid.fi/globalassets/dokumentit/fi/palvelut/kulutuksen-jatuotannon-liittaminen-kantaverkkoon/subsynchronous-oscillation-risk-of-wpps-connecting-to-finnish-series-compensated-network-white-paper.pdf>
- [22] D. Gros, M. Colombino, J.-S. Brouillon, and F. Dorfler, "The effect of transmission-line dynamics on grid-forming dispatchable virtual oscillator control," *IEEE Trans. Control Netw. Syst.*, vol. 6, no. 3, pp. 1148–1160, Sep. 2019, doi: [10.1109/TCNS.2019.2921347](https://doi.org/10.1109/TCNS.2019.2921347).
- [23] M. G. Dozein, A. M. De Corato, and P. Mancarella, "Virtual inertia response and frequency control ancillary services from hydrogen electrolyzers," *IEEE Trans. Power Syst.*, early access, Jun. 10, 2022, doi: [10.1109/TPWRS.2022.3181853](https://doi.org/10.1109/TPWRS.2022.3181853).
- [24] S. Shahil, W. Yan, P. Koralewicz, E. Mendiola, and V. Gevorgian, "A reversed impedance-based stability criterion for IBR grids," in *Proc. 21st Wind Solar Integr. Workshop*, The Hague, Netherlands, Oct. 2022, p. 8.
- [25] L. Yashen, J. H. Eto, B. B. Johnson, J. D. Flicker, R. H. Lasseter, H. N. Villegas Pico, G.-S. Seo, B. J. Pierre, and A. Ellis, "Research roadmap on grid-forming inverters," Nat. Renew. Energy Lab., Golden, CO, USA, Tech. Rep. NREL/TP-5D00-73476, 2020. [Online]. Available: <https://www.nrel.gov/docs/fy21osti/73476.pdf>
- [26] L. Fan, Z. Miao, S. Shah, P. Koralewicz, V. Gevorgian, and J. Fu, "Data-driven dynamic modeling in power systems: A fresh look on inverter-based resource modeling," *IEEE Power Energy Mag.*, vol. 20, no. 3, pp. 64–76, May 2022, doi: [10.1109/MPE.2022.3150827](https://doi.org/10.1109/MPE.2022.3150827).

- [27] J. Matevosyan, J. MacDowell, N. Miller, B. Badrzadeh, D. Ramasubramanian, A. Isaacs, R. Quint, E. Quitmann, R. Pfeiffer, H. Urdal, T. Prevost, V. Vittal, D. Woodford, S. H. Huang, and J. O'Sullivan, "A future with inverter-based resources: Finding strength from traditional weakness," *IEEE Power Energy Mag.*, vol. 19, no. 6, pp. 18–28, Nov. 2021, doi: [10.1109/MPE.2021.3104075](https://doi.org/10.1109/MPE.2021.3104075).
- [28] W. Du, F. K. Tuffner, K. P. Schneider, R. H. Lasseter, J. Xie, Z. Chen, and B. Bhattacharai, "Modeling of grid-forming and grid-following inverters for dynamic simulation of large-scale distribution systems," *IEEE Trans. Power Del.*, vol. 36, no. 4, pp. 2035–2045, Aug. 2021, doi: [10.1109/TPWRD.2020.3018647](https://doi.org/10.1109/TPWRD.2020.3018647).
- [29] X. Wang and F. Blaabjerg, "Harmonic stability in power electronic-based power systems: Concept, modeling, and analysis," *IEEE Trans. Smart Grid*, vol. 10, no. 3, pp. 2858–2870, May 2019.
- [30] T. Qoria, T. Prevost, G. Denis, F. Gruson, F. Colas, and X. Guillaud, "Power converters classification and characterization in power transmission systems," in *Proc. 21st Eur. Conf. Power Electron. Appl. (EPE ECCE Europe)*, Sep. 2019, pp. 1–10, doi: [10.23919/EPE.2019.8914783](https://doi.org/10.23919/EPE.2019.8914783).
- [31] Z. Li, P. Ponnaganti, F. Zhao, X. Wang, B. Bak-Jensen, S. Munk-Nielsen, and F. Blaabjerg, "Testing requirements and control strategies of next-generation grid emulator: A review," in *Proc. Int. Power Electron. Conf. (IPEC-Himeji ECCE Asia)*, May 2022, pp. 1560–1566, doi: [10.23919/IPEC-Himeji2022-ECCE53331.2022.9807056](https://doi.org/10.23919/IPEC-Himeji2022-ECCE53331.2022.9807056).
- [32] A. Hoke, P. Koralewicz, R. W. Kenyon, B. Wang, L. Yu, K. Kawamura, and J. Tan, "Stabilizing inverter-based transmission systems: Power hardware-in-the-loop experiments with a megawatt-scale grid-forming inverter," *IEEE Electrific. Mag.*, vol. 10, no. 3, pp. 32–44, Sep. 2022, doi: [10.1109/MELE.2022.3187634](https://doi.org/10.1109/MELE.2022.3187634).
- [33] A. Tayyebi, D. Groß, A. Anta, F. Kupzog, and F. Dörfler, "Frequency stability of synchronous machines and grid-forming power converters," *IEEE J. Emerg. Sel. Topics Power Electron.*, vol. 8, no. 2, pp. 1004–1018, Jun. 2020, doi: [10.1109/JESTPE.2020.2966524](https://doi.org/10.1109/JESTPE.2020.2966524).
- [34] L. S. Araujo, T. Caldognetto, D. Brandao, and P. Mattavelli, "Harmonic voltage synchronization using GPS modules for grid-connected power converters," *IEEE Open J. Power Electron.*, vol. 3, pp. 905–914, 2022, doi: [10.1109/OJPEL.2022.3222066](https://doi.org/10.1109/OJPEL.2022.3222066).
- [35] C. Li, Y. Huang, H. Deng, and X. Zhang, "Comparison on frequency stability of high inverter penetration power system with different grid-forming controls," in *Proc. Int. Conf. Power Energy Syst. Appl. (ICoPESA)*, Feb. 2022, pp. 374–380, doi: [10.1109/ICoPESA54515.2022.9754388](https://doi.org/10.1109/ICoPESA54515.2022.9754388).



HANNU LAAKSONEN (Member, IEEE) received the M.Sc. (Tech.) degree in electrical power engineering from the Tampere University of Technology, Tampere, Finland, in 2004, and the Ph.D. (Tech.) degree in electrical engineering from the University of Vaasa, Vaasa, Finland, in 2011. His employment experience includes working as a Research Scientist at the VTT Technical Research Centre of Finland and the University of Vaasa. He has previously worked as a Principal Engineer at ABB Ltd., Vaasa. He is currently a Professor of electrical engineering with the University of Vaasa. He is also a Research Team Leader and the Manager of the Smart Energy Master's Programme at the School of Technology and Innovations, Flexible Energy Resources, University of Vaasa. His research interests include the control and protection of low-inertia power systems and microgrids, active management of distributed and flexible energy resources in future smart energy systems, and future-proof technology and market concepts for smart grids.

• • •